Linking river-flood dynamics to hyperpycnal-plume deposits: Experiments, theory, and geological implications

Michael P. Lamb†, Brandon McElroy, Bryant Kopriva, John Shaw, and David Mohrig
Jackson School of Geosciences, University of Texas, 1 University Station C1100, Austin, Texas 78712-0254, USA

ABSTRACT

Turbid river plumes entering ocean or lake water of lesser density (i.e., hyperpycnal plumes) can plunge to form turbidity currents providing an important link between terrestrial sediment sources and marine depositional sinks. A leading hypothesis suggests that hyperpycnal-plume deposits accurately record the rising and falling discharge of a flooding river (in terms of sediment-size grading, bedform sequence, and deposit thickness), which, if correct, has significant implications for unraveling river dynamics, reservoir potential, and Earth history from marine-event beds. Herein, we present one of the first experimental flume studies aimed at testing this hypothesis. Results indicate that depth-averaged hyperpycnal-plume velocities can be uncorrelated or even anti-correlated with river discharge at certain seabed locations because of translation of the plunge point resulting from temporal variations in discharge and sediment concentration through the duration of a river flood. An advection length scale of settling sediment is found to be an important control on hyperpycnal-plume deposits, where coarse sediment (sand) is most likely to record multiple flow accelerations and decelerations related to plunge-point translation even for a river flood with a single-peaked hydrograph. In contrast, fine sediment (mud) is relatively insensitive to local plunge-point dynamics and is most likely to preserve directly rising and falling river discharge. Finally, it was found that the necessary fluvial sediment concentration to form a plunging plume can be much larger than the concentration typically used assuming density equivalence because of deposition upstream of the plunge point.

†E-mail: mpl@gps.caltech.edu; Current address: Division of Geological and Planetary Sciences, California Institute of Technology, MC 170-25, 1200 E. California Boulevard, Pasadena, California 91125, USA

INTRODUCTION

Turbidity currents are a primary mechanism for source-to-sink sediment transport on continental margins, and their deposits are important reservoirs and records of Earth history. Many models for turbidity-current generation rely on mass failures of steep submarine slopes such as continental slopes, submarine canyons, and delta fronts (e.g., Normark et al., 1993). Turbidity currents, however, can also be generated by turbid river plumes that enter a standing body of water of lesser density (e.g., Wright et al., 1986). These so-called hyperpycnal river plumes are important for transporting and depositing sediment across continental shelves and slopes, and potentially for incising submarine canyons. Moreover, they are one of the most direct links between terrestrial sediment sources and marine depositional sinks, and their deposits are thought to contain a record of river floods through varying climatic and tectonic regimes (Mulder et al., 2003). Because hyperpycnal events occur infrequently and the flows and deposits are difficult to sample, it is not yet known how river-flood dynamics are linked to hyperpycnal-plume deposits.

Assuming density equivalence and using a rating curve technique, many small- and medium-sized rivers have been argued capable of generating hyperpycnal plumes on annual to decadal time scales (Mulder and Syvitski, 1995). Others have suggested that they can occur more frequently if mixing between river plume and ocean water is considered (Parsons et al., 2001; Felix et al., 2006). By definition hyperpycnal plumes occur where the density of the turbid river plume exceeds the density of the ambient fluid. However, in order for a hyperpycnal plume to plunge and form a turbidity current, the basin must be deep enough for the turbid water column to become unstable and collapse beneath the ambient fluid (Akiyama and Stefan, 1984).

Although plunging river plumes have been documented off the Huanghe River, China (Wright et al., 1990); Sepik River, Papua New Guinea (Kineke et al., 2000); and rivers in Taiwan (Dadson et al., 2005), New Zealand (Hicks et al., 2004), and California (Johnson et al., 2001; Warrick and Milliman, 2003), few studies have directly linked hyperpycnal-plume deposits to river-flood dynamics. The leading hypothesis is that hyperpycnal-plume velocities scale with the discharge of the flooding river and that their deposits record the history of the flood event in terms of grain-size grading patterns, bedform sequences, and deposit thicknesses (Fig. 1A) (Mulder et al., 2003). As an example, Figure 1A shows a simple hypothetical flood where the discharge first increases and then decreases in time. A corresponding hyperpycnal-plume deposit might contain ripples in very fine sand, followed by higher energy upper plane-bed in fine sand, capped by ripples in very fine sand (Fig. 1B). Mulder et al. (2001a, 2001b) interpreted such

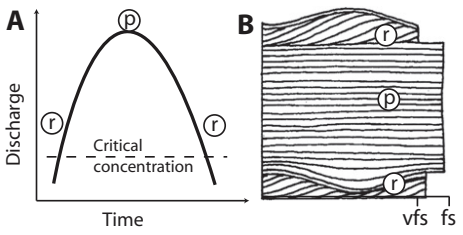

Figure 1. (A) Hypothetical river flood showing discharge through time. Once the critical sediment concentration (the concentration at which the bulk density of a turbid freshwater plume equals the density of seawater) is exceeded, it is typically assumed that hyperpycnal-plume velocity will track the rise and fall of river discharge. (B) Schematic of an ancient event bed interpreted to be a hyperpycnal-flow deposit by Lamb et al. (2008) that tracks a river flood resulting in ripples (r) in very fine sand (vfs) in the rising limb, plane bed (p) in fine sand (fs) at the flood peak, and ripples in vfs as the flood wanes. The vertical axis is deposit thickness and the horizontal axis is grain size.

GSA Bulletin; September/October 2010; v. 122; no. 9/10; p. 1389–1400; doi: 10.1130/B30125.1; 15 figures; 1 table.

reverse-to-normally graded beds in the Mediterranean to be deposits of hyperpycnal plumes that tracked the history of river flooding. Lamb et al. (2008) and Myrow et al. (2008) proposed a similar link to river floods from ancient deposits that record waxing to waning flow conditions. In their review, Mulder et al. (2003) suggested that reverse-to-normal grading might be one of the dominant signatures of hyperpycnal-plume deposits, although reflections due to complex topography (e.g., Lamb et al., 2004), retrogressive failure (e.g., van den Berg et al., 2002), and other mechanisms (e.g., Best et al., 2005) might also create such deposits.

The hypothesis of Mulder and others, if correct, is powerful because it indicates that the temporal history of river floods can be inferred from their marine deposits, of which there is a rich record. However, normal river flow must transition through a backwater zone, depth-limited plume, and plunging plume before becoming a turbidity current (Fig. 2). The backwater zone extends from the shoreline to some distance upstream ($x < x_s$, where $x_s = 0$ is the shoreline location) where river flow is affected by the standing ocean water beyond the shoreline (Henderson, 1966). The depth-limited plume occurs beyond the shoreline where the flow does not have the necessary depth to plunge ($x_s < x < x_p$, where x_p is the location of the plunge point) (Akiyama and Stefan, 1984). And the plunging plume is a zone of collapse and acceleration of an underflow ($x_p < x < x_d$, where x_d is the downstream extent of plunging). Lamb and Mohrig (2009) used a simple numerical model to show that these transitional zones can significantly affect the transfer of momentum from normal-river flow to the turbidity current because the boundaries of these zones migrate during the course of a flood. This behavior will likely result in a wide range of depositional characteristics along the bed including some positions that do not track the rising and falling discharge of a river flood.

In this paper, we present a set of two-dimensional (2-D) physical experiments aimed at evaluating how hyperpycnal-plume dynamics and deposits respond to changes in inlet fluvial discharge and sediment concentration. The experiments were designed to investigate the depth-limited and plunging plumes (Fig. 2), and the translation of the plunge point as a function of river boundary conditions. The ultimate goal is to provide data to work toward developing an accurate inverse model in which river-flood dynamics might be determined from hyperpycnal-plume deposits. First, we describe the experimental setup and measurement scheme. Second, we present results for controls on plunging and the effects of inlet fluvial discharge and sediment concentration on the plume dynamics and deposits. Finally, we analyze our results and discuss their implications at field scale.

EXPERIMENTAL SETUP

The experiments were performed in a 3-m-long tilted ramp set inside a 7-m-long, 0.24-m-wide flume filled with fresh tap water (Fig. 3). The tilted ramp had a smooth Plexiglas bed at the beginning of each experiment. A slurry was introduced to the headbox by mixing freshwater from a constant-head tank with dry sediment from a vibrating-screw sediment feeder. This mixture filled and overspilled the ~50-mm-deep headbox ensuring a well-mixed inlet flow that was spread evenly across the width of the flume. The standing water level in the flume was set to slightly below the elevation of the headbox through use of a standpipe. The temperature of water in the flume and the input slurry were measured before each experiment, and density contrasts due to temperature were negligible. The inlet open-channel flows were <10 mm deep, and because of the steep and smooth bed of the flume, they were supercritical. Most natural rivers are subcritical upon entering the ocean and do not form a hydraulic jump (e.g., Fig. 2). To make our inlet conditions more realistic, a small (~5-mm-high) step was fastened to the bed to force a hydraulic jump at the approximate location of maximum flooding from the standing water. Therefore, the test section analyzed herein is the region of subcritical open-channel flow from the hydraulic jump ($x = x_s = 0$) to the end of the test section ($x = 2.5$ m) (Fig. 3).

Seven experiments were performed with different initial sediment concentrations and discharges (Table 1). All experiments used the same crushed silica for sediment ($D_{84} = 43$ μm,

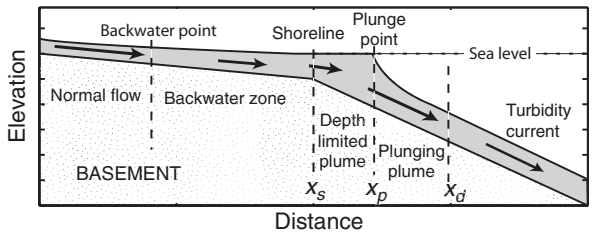

Figure 2. Schematic of the major zones of a hyperpycnal river plume. Normal river-flow transitions through a backwater zone, a depth-limited plume between the shoreline ($x = x_s$) and the plunge point ($x = x_p$), and a plunging plume before becoming a turbidity current ($x > x_d$). The length of the arrows represents relative flow velocities.

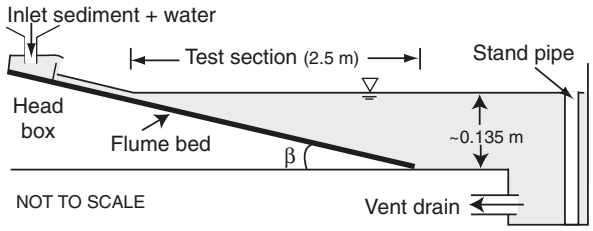

Figure 3. Drawing of the experimental flume. Sediment and water were mixed into a slurry and entered the flume through the headbox. Measurements of the depth-limited plumes, plunging plumes, and turbidity currents were made in a 2.5-m-long test section along a ramp of slope S = tan β. The backwater zone of Figure 2 was not analyzed in these experiments. The water level was held constant through use of a standpipe and turbid water was vented out of the system at the downstream end.

TABLE 1. MEASURED EXPERIMENTAL VALUES AT THE INLET, PLUNGE POINT, AND DOWNSTREAM OF PLUNGING. SEE APPENDIX FOR NOTATION

	Experiment						
	1	2	3	4	5	6	7
q_0 (m²/s)	0.0025	0.0043	0.0012	0.0016	0.0033	0.0043	0.0043
c_0 (%)	0.12	0.36	2.0	0.54	0.54	0.54	1.0
S	0.1	0.05	0.05	0.05	0.05	0.05	0.05
x_p (m)	0.6	2.1	1.0	1.5	1.7	1.8	1.5
h_p (mm)	150	110	50	70	75	95	65
c_p (%)	0.06	0.24	1.2	0.28	0.38	0.34	0.8
D_{50p} (μm)	6.7	15.2	9.0	10.4	10.4	9.2	12.0
q_d (m²/s)	0.0041	0.0063	0.0017	0.0025	0.0036	0.005	0.0046
x_d (m)	1.4	2.4	1.4	1.8	2.1	2.1	2.0
h_d (mm)	120	90	41	55	55	70	55
c_d (%)	0.05	0.11	1.0	0.19	0.27	0.26	0.7
D_{50d} (μm)	6.1	9.4	9.3	8.1	8.9	7.9	9.4

D_{50} = 21 µm, D_{16} = 3 µm, where the subscript denotes the percentage of grains with a nominal diameter finer than the indicated size with a density of ρ_s = 2650 kg/m^3. The test section for the first experiment had a bed slope, S = tan β (Fig. 3), of 10%, and the remaining six experiments had S = 5%. The inlet volumetric sediment concentration (c_0) and volumetric water discharge per unit width (q_0) were held constant during the course of each experiment lasting ~60 min. Downstream of the test section the turbidity currents were vented out of the system in the tailbox. The stream-wise location of the plunge point stabilized within ~2 min of the beginning of each experiment, after which each flow reached a quasi–steady state, where properties such as thickness and velocity changed little at any particular location except in response to slow aggradation of the bed. It was during this quasi–steady state that all measurements were made.

The stream-wise profiles of flow thickness were measured from digitized photographs taken immediately following stabilization of the plunge point (e.g., Fig. 4). In addition, a set of seven vertically stacked siphons with inside diameters of 4 mm was used to extract samples for sediment concentration and grain-size analysis. For each experiment, ~500 ml of sediment-laden water were collected over the course of ~5 min at two locations, one at the plunge point ($x = x_p$) and one just downstream of the plunging zone ($x = x_d$, Fig. 2). The flow velocity in the siphons was set to be near the depth-averaged flow velocity in the test section by adjusting the elevation of the siphon outlets (i.e., the head gradient) to minimize sampling bias (Federal Interagency Sedimentation Project, 1941). Errors in suspended sediment concentration associated with siphon intake velocities that differ from the free-stream velocity are a function of particle inertia and are small for particles that range in size from mud to very fine sand (Winterstein and Stefan, 1983). Based on analyses of errors in suspended sediment concentration by the Federal Interagency Sedimentation Project (1941), we estimate that error in suspended sediment concentration for our experiments was less than 5% of the actual concentration value. Nominal diameters for particles collected in the siphon samples were measured using a Horiba LA-300 laser particle-size analyzer, and sediment concentrations were determined by weighing the samples. Velocity profiles were taken at four to eight locations in the stream-wise direction using a Nortek acoustic Doppler profiler (ADP). These profiles were collected at 4 Hz and averaged over ~120 s. The ADP has a vertical resolution of 9 mm and a blanking distance of ~40 mm that prevented measurement of the uppermost parts of flows. The depth and location of the plunge point were recorded visually near the beginning, middle, and end of each experiment.

Depth-averaged velocity, U, depth-averaged sediment concentration, c, and depth-averaged median grain size were calculated at each profile station using a linear interpolation between data points and the trapezoid method of finite integration. Depth-averaged flow velocities upstream of the plunge point were calculated from continuity (i.e., $U = q_0/h$) instead of from the ADP profiles because of the ADP's relatively large blanking distance. Downstream of plunging, velocities were set to zero above the visualized height of the turbidity current before integrating when the zero point in the velocity profile was not measured due to the ADP blanking distance.

After each experiment was completed, the standing water in the flume was allowed to clarify for one to three days to facilitate measurements of the experimental deposit. Bed topography was scanned using a displacement laser with 0.3-mm vertical resolution attached to an automated cart that was programmed to produce a 2-mm × 2-mm resolution grid over the test section. A deposition rate was calculated for each experiment from the centerline topographic scan of the deposit at the end of each experiment divided by the duration of the experiment. The composition of the deposit was characterized by five samples collected every 0.5 m along the centerline and analyzed using the laser particle sizer. The sediment deposit was removed prior to each subsequent experiment.

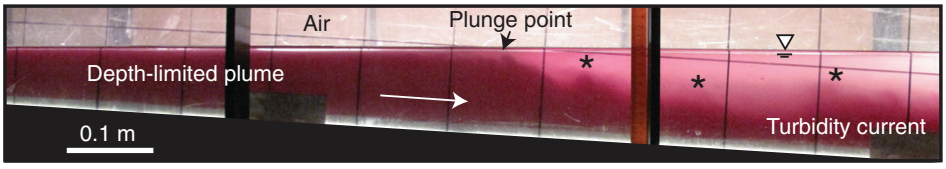

Figure 4. Photograph from Experiment 7 showing the depth-limited plume collapsing at the plunge point to form a turbidity current. Kelvin-Helmholtz billows (marked by asterisks) visible in the plunging and turbidity-current zones entrained ambient fluid into the hyperpycnal plumes. The grid on the flume wall was 0.1 m × 0.1 m.

RESULTS

During each experiment the turbid flow encompassed the entire water column from the beginning of the test section ($x = x_s = 0$) to the plunge point (Figs. 4, 5A, and 6A) forming a depth-limited plume. Downstream of the plunge point, the flows collapsed by several tens of millimeters (Table 1) over a distance of ~0.5 m and ran out as turbidity currents of near constant thickness. The variation in thickness evident in the turbidity current profiles is due to mixing (e.g., Kelvin-Helmholtz billows; Turner, 1973) recorded in the digitized photographs (e.g., Fig. 4). Despite a near quasi–steady state, the plunge point tended to oscillate in the stream-wise direction by ~0.1 m over a time scale of a few tens of seconds in response to mixing and collapse in the plunge zone. The plunge point also translated downstream by ~0.2 m over the course of an experiment due to deposition of sediment on the bed.

The plunge point had a significant influence on the downstream profiles of velocity (Figs. 5B and 6B). In the depth-limited plume, the flows decelerated spatially, reaching their minimum depth-averaged velocity at the plunge point (Figs. 5B and 6B). Significant spatial acceleration occurred in the plunging plume (e.g., Fig. 7C), increasing depth-averaged velocities from those at the plunge point by up to a factor of 2 (Table 1). In the turbidity current zone downstream of the plunging plume, flow velocities were approximately uniform.

The measured sediment concentrations and suspended particle sizes were relatively constant in the vertical dimension at the plunge point (Figs. 7A and 7B). In contrast, sediment concentration and grain size generally increased toward the bed in the plunging and turbidity-current zones. In addition, the flow at the plunge point contained more sediment and coarser particles than farther downstream in the collapsed plume because of sedimentation (Table 1, Fig. 7). In some cases, grain sizes and concentrations measured from the lowest-most siphon were smaller than samples higher in the water column (e.g., Figs. 7A and 7B), which might have been caused by fouling of the siphon from being too close to the bed.

Upstream of the test section ($x < x_s = 0$), the sediment transport capacity exceeded the sediment supply, such that there was no deposition of sediment. In the test section, however, rapid deceleration of flow in the depth-limited plume decreased entrainment and forced deposition. The deposition rate increased from zero to several tens of millimeters per hour over the first 0.5–0.75 m of the test section, and then slowly decreased in the downstream direction (Figs. 5C

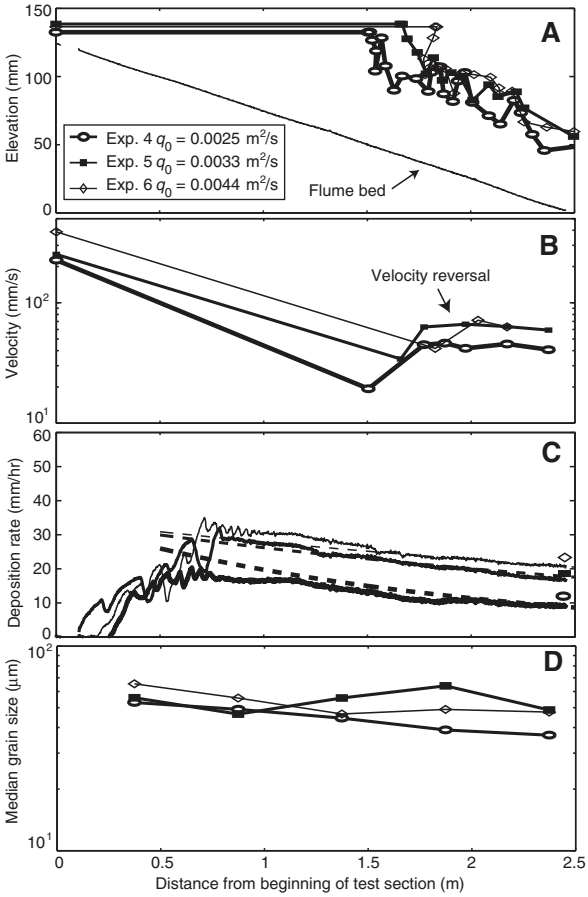

Figure 5. Measurements from Experiments 4, 5, and 6 showing the effect of inlet discharge. All cases had the same sediment concentration of 0.54%. (A) Elevation profiles of the top of the turbid hyperpycnal plume versus downstream distance within the test section extracted from digitized photographs taken after stabilization of the plunge point in each experiment. (B) Depth-averaged velocity as a function of distance. The velocity upstream of the plunge point was calculated from continuity ($U = \frac{q_0}{h}$), and the velocity downstream of the plunge point was measured using the acoustic Doppler profiler. Note the region where changes in local flow velocity were anti-correlated with changes in inlet discharge is marked "Velocity reversal." (C) Deposition rate as a function of distance calculated from the centerline thickness of each final deposit divided by the duration of each experiment. Note the ripples in the upstream portion of the test section. The dashed lines are predictions using Equation (15) as discussed in the Analysis Section. (D) Median grain size of the final deposit as a function of distance downstream.

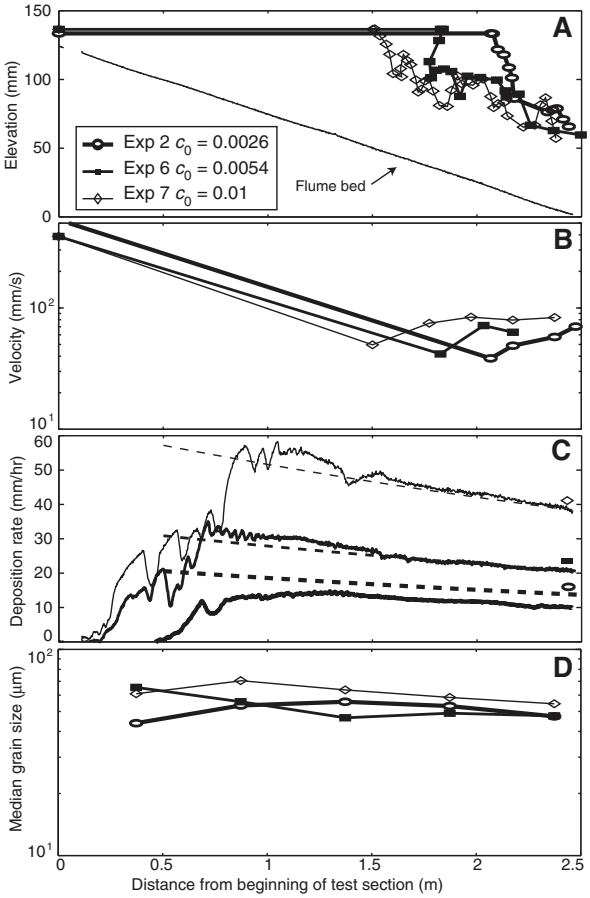

Figure 6. Measurements from Experiments 2, 6, and 7 showing the effect of inlet sediment concentration. All cases had the same inlet discharge of 0.0044 m^2/s. (A) Elevation profiles of the top of the turbid hyperpycnal plume extracted from digitized photographs taken after stabilization of the plunge point in each experiment. (B) Depth-averaged velocity as a function of distance. The velocity upstream of the plunge point was calculated from continuity ($U = \frac{q_0}{h}$), and the velocity downstream of the plunge point was measured using the acoustic Doppler profiler. (C) Deposition rate of sediment as a function of distance calculated from the centerline thickness of each final deposit divided by the duration of each experiment. The dashed lines are predictions calculated using Equation (15) as discussed in the Analysis Section. (D) Median grain size of the final deposit as a function of distance downstream.

and 6C). Although flows accelerated through the plunge zone, the deposition rate remained positive. Evidently the increase in entrainment rate of sediment from the bed during plunging was not sufficient to counteract the fallout of sediment.

The median grain size of the bed material tended to decrease in the downstream direction for some experiments, but there is scatter (Fig. 6D). The deposits were significantly coarser than the input grain-size distribution (D_{50} = 21 μm) and the median particle sizes in the flows (D_{50} ~10 μm) (Table 1). Figure 8 shows an example of the dramatic coarsening of the bed and fining of the flow due to preferential deposition of coarse sediment.

All of the experiments generated ripple-like bedforms in the upstream portions of the test

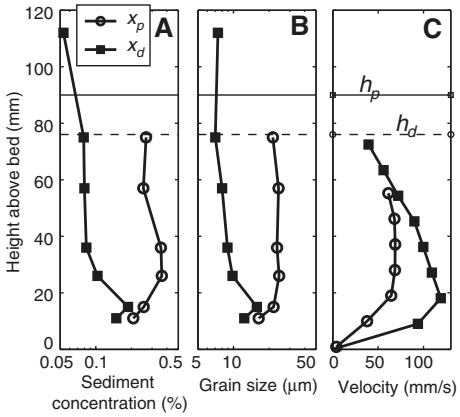

Figure 7. Vertical profiles of (A) sediment concentration, (B) median grain size, and (C) stream-wise flow velocity from Experiment 2 at the plunge point, x_p = 2.2 m, and downstream of the plunging zone, x_d = 2.5 m. Experiment 2 is shown because it had the greatest plunge-point depth (except for Experiment 1, which had a different bed slope) and therefore the greatest vertical data density. The dashed horizontal line shows the visualized height of turbid flow at the plunge point, h_p, and the solid horizontal line shows the visualized height of turbid flow (i.e., turbidity current) downstream of plunging, h_d.

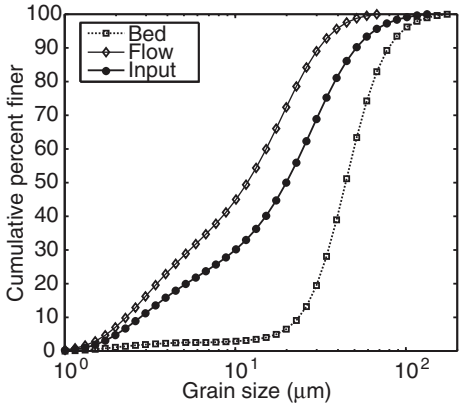

Figure 8. Grain-size distributions from Experiment 4 for the final bed deposit at x = 2.0 m, the flow ~25 mm above the bed in the plunging zone at x = 1.8 m, and the input sediment.

section (Figs. 5C and 6C) where velocities were large (Figs. 5B and 6B). The ripples diminished in height and wavelength downstream, usually transitioning to lower planar bed upstream of the plunge point. Despite acceleration upon plunging, ripples never reformed downstream of the plunge point.

ANALYSIS

Criteria for Plunging

Theoretical modeling by Akiyama and Stefan (1984) suggests that plunging of river plumes can be described by the densimetric Froude number where

$$F_d = \frac{q}{\sqrt{\Delta\rho g h^3/\rho_a}} \quad (1)$$

for dilute flow ($c << 1$) and $q = Uh$ is the discharge per unit width, h is the flow depth, $\Delta\rho$ is density of the current in excess of the ambient fluid density ρ_a, and g is the acceleration due to gravity. For the case of a fresh turbid plume,

$$\Delta\rho = \rho_w(1 + Rc) - \rho_a, \quad (2)$$

where ρ_w is the density of fresh water, R is the submerged specific density of sediment ($R = \frac{\rho_s - \rho_w}{\rho_w}$ and ρ_s is the density of sediment), and c is the depth-averaged volumetric concentration of sediment.

There are two necessary conditions that must be satisfied for a hyperpycnal plume to plunge. The first is that the concentration of sediment must exceed a critical concentration to create a density excess with respect to the ambient fluid. The critical concentration for plunging, c_c, can be found by setting $\Delta\rho = 0$ in Equation (2) as,

$$c_c = \frac{1}{R}\left(\frac{\rho_a}{\rho_w} - 1\right). \quad (3)$$

The second necessary condition is that depths in the basin must be large enough for the turbid flow to become unstable. The necessary depth for plunging, h_p, can by found be rearranging Equation (1) as

$$h_p = \left(\frac{q_p^2}{(\Delta\rho/\rho_a) g F_{dp}^2}\right)^{1/3}, \quad (4)$$

where F_{dp} is the value of the densimetric Froude number at the plunge point ($x = x_p$, Fig. 2) and q_p is the discharge at the plunge point.

Parker and Toniolo (2007) showed that the densimetric Froude number at the plunge point, F_{dp}, and the densimetric Froude number downstream of plunging, $F_{dd} = F_d(x = x_d)$, are functions only of a coefficient of mixing,

$$\gamma \equiv \frac{q_d}{q_p} - 1, \quad (5)$$

where q_d is the discharge of the collapsed current at $x = x_d$ (Fig. 2), although bed slope might also play a role (Dai and Garcia, 2009). Previous flume experiments indicate that γ ranges from 0.1 to 0.3 (Itakura and Kishi, 1979; Farrell, 1986; Lee and Yu, 1997; Toniolo et al., 2007). Using $\gamma \approx 0.17$ (Lee and Yu, 1997), for example, the model of Parker and Toniolo (2007) indicates that F_{dp} = 0.5, F_{dd} = 1, and the ratio of the downstream flow thickness to that at the plunge point is h_d/h_p = 0.75. Thus, the plume is expected to occupy the entire water column until the densimetric Froude number drops below ~0.5. At this point, the plume collapses to a flow depth about three-quarters as thick and to a densimetric Froude number near the critical value of unity. The stream-wise length over which plunging occurs ($L_p = x_d - x_p$) is thought to scale as $L_p = Ah_p$, where A is a constant greater than unity (e.g., Lee and Yu, 1997).

Our experimental results can be used to test these predictions. The measured flow discharge downstream of plunging was typically greater than the discharge at the plunge point as expected from entrainment of ambient fluid during plunging (Fig. 9A). The data are scattered, however, due to error in calculating discharge from the ADP, which could not sample within 40 mm of the free surface. We measured the total length of the plunging zone ($L_p = x_d - x_p$) using flow visualization to be ~0.3–0.8 m in different experiments, corresponding roughly to ~5 h_p (Fig. 9B). A value of $\gamma \approx 0.2$ seems reasonable for entrainment over this distance (Fig. 9C). Continued entrainment downstream of plunging caused $\gamma > 0.2$ in the turbidity current zone (Fig. 9A).

For $\gamma = 0.2$, the Froude numbers at the plunge point and downstream of the plunging zone are predicted to be F_{dp} = 0.45 and F_{dd} = 1.1, and the plume is expected to collapse to h_d/h_p = 0.7 (Parker and Toniolo, 2007). In our experiments, the plunge-point depths ranged from ~50 to 110 mm and match the prediction of F_{dp} = 0.45 well (Fig. 10A). In addition, the plumes typically collapsed to $h_d = 0.7h_p$ (Fig. 10B) and F_{dd} = 1.1 at the end of the plunge zone (Fig. 10A) as predicted by theory (Parker and Toniolo, 2007).

Effect of Deposition on Plunging Criteria

It is common to assume that hyperpycnal river plumes retain their sediment in suspension during passage from the shoreline to the plunge point (e.g., Mulder and Syvitski, 1995). This assumption simplifies the necessary condition on concentration so that plunging occurs when the *fluvial* suspended sediment concentration exceeds c_c (Equation 3). However, the second necessary condition for plunging of a critical depth (Equation 4) allows the formation of a depth-limited plume (Fig. 2). In our ex-

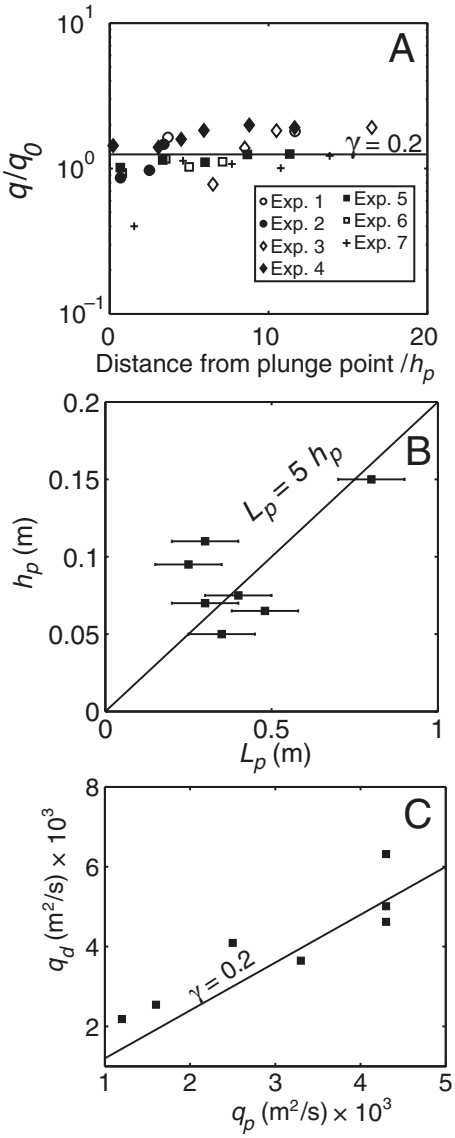

Figure 9. (A) Discharge of turbid flow, q, normalized by the input discharge, q_0, versus the distance downstream from the plunge point normalized by the plunge-point depth, h_p. In our experiments, the discharge at the plunge point was equal to the input discharge ($q_p = q_0$). In general, the discharge downstream of the plunge point was greater than the inlet due to fluid entrainment, and an entrainment coefficient $\gamma = 0.2$ is shown for reference. There is significant scatter due to error in calculating discharge because the acoustic Doppler profiler could not sample the upper ~40 mm of the water column (e.g., Fig. 7C). (B) Plunge-point depth, h_p, versus measured length of the plunge zone, L_p. The error bars are ±0.1 m owing to oscillations of the plunge point. (C) Measured discharge at the downstream boundary of the plunging zone, q_d, versus discharge at the plunge point, q_p. Also shown is the prediction for $\gamma = 0.2$.

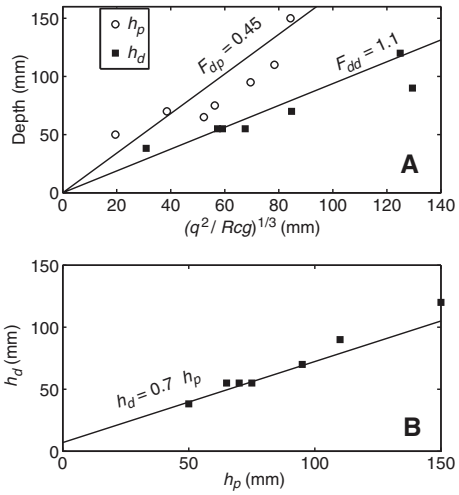

Figure 10. (A) Measured depth of turbid flow at the plunge point, h_p, and downstream of plunging, h_d, versus the predicted length scale for a constant value of the densimetric Froude number, F_d, given by Equation (1). The two lines represent predictions using Equation (4) and $\gamma = 0.2$ in Parker and Toniolo (2007), which yields $F_d = F_{dp} = 0.45$ for the plunge point and $F_d = F_{dd} = 1.1$ for downstream of plunging. (B) The depth of turbid flow downstream of plunging, h_d, versus that at the plunge point, h_p. The prediction of $h_d = 0.7\ h_p$ is from Parker and Toniolo (2007) for $\gamma = 0.2$.

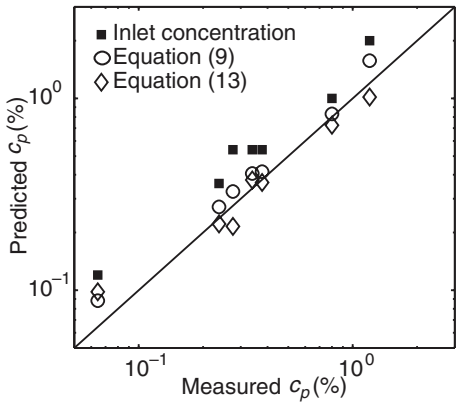

Figure 11. Predicted versus measured depth-averaged sediment concentration at the plunge point. The model predictions are (1) assuming that the plunge-point concentration equals the inlet concentration at the river mouth, (2) reducing the plunge-point concentration from that at the inlet due to the observed deposition rate following Equation (9), and (3) reducing the plunge-point concentration from that at the inlet due to settling of sediment following Equation (13). The solid line is a 1:1 correlation.

periments, deposition within the depth-limited plume reduced the sediment concentration at the plunge point by up to a factor of 2 from its original value at the fluvial inlet (Fig. 11).

For quasi–steady flow, the rate of deposition, $\frac{d\eta}{dt}$, can be calculated from sediment continuity as

$$(1-\lambda_p)\frac{d\eta}{dt} = -\frac{dq_s}{dx}, \tag{6}$$

where q_s is the volumetric sediment flux per unit width, and λ_p is the bed porosity. To analyze sediment deposition in the depth-limited plume, we calculate the divergence in sediment flux (i.e., $-\frac{dq_s}{dx}$) by assuming suspended sediment as

$$\frac{dq_s}{dx} \approx q\frac{c_p - c_s}{x_p - x_s}, \tag{7}$$

where c_p is the depth-averaged sediment concentration at the plunge point ($x = x_p$), and c_s is depth-averaged concentration at the river mouth ($x = x_s$), which for our experiments is equivalent to the inlet sediment concentration (i.e., $c_s = c_0$) because there was complete sediment bypass in the fluvial zone ($x < x_s$). The distance between the shoreline and the plunge point can be calculated using geometry by knowing the downstream slope of the basin and the plunge-point depth as

$$x_p - x_s = \frac{(h_p - h_s)}{S}, \tag{8}$$

where h_s is the depth at the shoreline. If $h_p >> h_s$, as it was in our experiments, then combination of Equations (6–8) results in

$$c_p = c_s - (1-\lambda_p)\frac{d\eta}{dt}\frac{h_p}{qS}. \tag{9}$$

Equation (9) shows that the sediment concentration at the plunge point is reduced from that at the river mouth because of deposition within the depth-limited plume. The magnitude of sediment loss is larger for greater plunge depths, smaller discharges, and smaller bed slopes. This last relationship occurs because for lower bed-gradients the plunge point is pushed farther seaward providing more bed area over which deposition takes place.

Equation (9) was used to make predictions of the sediment concentration at the plunge point in our experiments using the spatially averaged deposition rates measured from the bed surveys. The bed porosity was assumed to be $\lambda_p = 0.5$ based on tests of similar sediment allowed to

settle for one to three days in a graduated cylinder. These predictions are about half the value of the inlet concentration and match well the observed concentrations (Fig. 11).

The concentration at the plunge point can also be found from sediment continuity by calculating the sediment flux gradient as the difference between the entrainment of sediment from the bed, ew_s, and the near-bed settling flux of sediment, $c_b w_s$,

$$\frac{dq_s}{dx} = w_s\left(e - c_b\right), \tag{10}$$

where c_b is the near-bed sediment concentration, w_s is the settling velocity, and e is a dimensionless entrainment parameter (Smith and Mclean, 1977; García and Parker, 1991). Due to the small flow velocities in our experiments, it is reasonable to assume that entrainment from the bed was negligible ($e = 0$). Setting $e = 0$ in Equation (10), and applying the definitions $q_s \equiv cq$ and $r_0 \equiv \frac{c_b}{c}$ (where $r_0 \geq 1$ is a parameter that describes the vertical sediment stratification [Parker et al., 1987] that can vary by about a factor of 2 in turbidity currents [Garcia, 1994]) results in

$$\frac{dc}{dx} = \frac{-r_0 w_s c}{q}. \tag{11}$$

If r_0, w_s, and q can be assumed constant in x, then the solution to Equation (11) subject to the boundary condition $c_s = c(x = x_s = 0)$ is found analytically to be

$$c = c_s \exp\left(\frac{-r_0 w_s}{q} x\right). \tag{12}$$

Equation (12) describes the exponential decay of sediment concentration in the downstream direction due to settling. Solving Equations (8) and (12) at the plunge point,

$$c_p = c_s \exp\left(\frac{-r_0 w_s h_p}{qS}\right), \tag{13}$$

indicates that the reduction in sediment concentration due to settling is greatest for large settling velocities, small fluid discharges, and small bed slopes, similar to Equation (9). To evaluate Equation (13) for our experiments, we set r_0 = 1.5 from examining the observed concentration profiles (e.g., Fig. 7A) and calculate $w_s = 4.4 \times 10^{-4}$ m/s for D_{50} = 21 μm sediment using Stokes' Law. In addition, like Equation (9), Equation (13) also shows good agreement with the measured plunge-point concentrations (Fig. 11). Thus, the sediment concentration at the plunge point was reduced from the input fluvial concentration due to the passive rainout of sediment within the depth-limited plume (Equation 13) that resulted in bed deposition (Equation 9).

Effect of Inlet Discharge on Flow Dynamics

Hyperpycnal flows with larger discharges or smaller sediment concentrations are expected to plunge at greater depths and produce thicker turbidity currents (Equation 4). In a basin that deepens seaward with a gradient S, a change in plunge depth, Δh_p, should produce downstream translation of the plunge point and expansion of the depth-limited plume by a distance $\Delta h_p/S$. In addition, using continuity, $q = Uh$, and Equation (1), it can be shown that

$$U = \left(\left(\Delta\rho/\rho_a\right) g F_d^2 q\right)^{1/3}. \tag{14}$$

Equation (14) predicts that, for all other things equal and constant F_d, higher discharge and higher concentrated flows are expected to have faster velocities at the plunge point and downstream of the plunge zone.

The effect of changing inlet fluvial discharge can be examined by comparing Experiments 4 through 6 where all other parameters including inlet sediment concentration (c_0 = 0.54%) were held constant (Table 1). An increase in discharge of ~75% between Experiments 4 and 6 produced a change in plunge-point depth from 70 to 95 mm (Fig. 5). This in turn caused the plunge point to translate basinward by ~0.5 m (i.e., $\Delta h_p/S$ = 0.025 m/0.05).

In general, higher discharge flows had thicker turbidity currents (Fig. 5A) and larger velocities throughout the test section (Fig. 5B) as expected from Equations (4) and (14). But, because the plunge point was free to move, the increase in discharge produced a decrease in local velocity at some locations above the bed. For example, at x = 1.8 m, the velocity was ~45 mm/s for the low discharge case (Experiment 4: q_0 = 0.0025 m^2/s), it increased to 64 mm/s for the middle discharge case (Experiment 5: q_0 = 0.0033 m^2/s), and then dropped to its lowest value of 40 mm/s for the high discharge case (Experiment 6: q_0 = 0.0044 m^2/s). These results suggest that local hyperpycnal-plume velocities can be correlated or anti-correlated with changes in river discharge depending on the particular location at the seabed with respect to the location and translation length of the plunge point during a flood event.

Effect of Inlet Sediment Concentration on Flow Dynamics

Experiments 2, 6, and 7 were designed to investigate the effect of variable inlet sediment concentration on plunging dynamics and deposits while holding the discharge constant (Table 1 and Fig. 6). As expected from Equation (4), larger sediment concentrations corresponded to shallower plunge depths, and this produced smaller depth-limited plumes with plunge points closer to the shoreline. For example, the inlet sediment concentration was increased by a factor of 4 between Experiments 2 and 7, which caused the plunge depth to decrease from ~110–65 mm and the plunge point to translate upstream by ~0.7 m (Fig. 6A). In general, flows with higher sediment concentration had thinner (Table 1) and faster (Fig. 6B) turbidity currents, consistent with Equations (4) and (14), although there was variability in thickness due to Kelvin-Helmholtz billows (Figs. 6A and 4).

Despite having the same inlet discharge, the downstream trends in velocity were different for Experiments 2, 6, and 7 because of translation of the plunge point and the dependence of turbidity-current velocity on sediment concentration (Equation 14). In the depth-limited plume, the open-channel flow velocities should have been the same between the three cases, but were not (Fig. 6B) because of slight differences in the water surface elevation (Fig. 6A) due to small errors in calibrating the standpipe (Fig. 3). This notwithstanding, it is clear that downstream of the plunge points (x > 1.5 m), the higher concentrated flows resulted in faster velocities independent of changes in discharge. These results indicate that hyperpycnal-flow velocity in the plunging and turbidity current zones can be uncorrelated to inlet discharge if fluvial sediment concentration varies independent of discharge.

Coupling Flow Dynamics to Deposits

Despite the complex response of flow velocity to changes in inlet discharge and sediment concentration, the deposition rate and grain sizes seemed to respond to the input conditions in a more straightforward way. In general, the experimental flows with larger discharges for the same sediment concentration resulted in a greater deposition rate (Fig. 5C) and a coarser deposit (Fig. 5D) everywhere except within the first ~0.6 m of the test section. Likewise, experiments with larger inlet sediment concentrations and the same discharge produced a greater deposition rate (Fig. 6C) and a coarser deposit (Fig. 6D). The ripples that formed in the upstream portions of the test section tended to be larger in the higher discharge and higher sediment concentration cases. Importantly, there were no changes in deposition rate, median grain size, or bedform geometry across the transition from decelerating to accelerating flow at the plunge point. Evidently, the deposit was more sensitive to inlet conditions than plunge-point dynamics.

From inspection of Equations (6) and (10) one might expect smaller deposition rates with larger discharges because the entrainment rate e scales nonlinearly with flow velocity (Smith and Mclean, 1977; García and Parker, 1991). However, where e is negligible, the deposition rate can increase with discharge because a larger velocity results in faster advection of sediment downstream, producing larger near-bed sediment concentrations and higher settling fluxes everywhere. This can be seen by combining Equations (6), (10), and (12),

$$(1-\lambda_p)\frac{d\eta}{dt} = r_0 w_s c_s \exp\left(\frac{-r_0 w_s}{q}x\right). \quad (15)$$

Equation (15) illustrates that, if e is negligible and r_0 and w_s are constant, the deposition rate is a function of the inlet fluvial sediment concentration and discharge only, and it is independent of any local changes in flow velocity or sediment transport capacity due to plunge-point dynamics.

The predictions of Equation (15) are shown as dashed lines on Figures 5C and 6C using the experimental inlet conditions of c_0 and q_0 (Table 1). The theoretical results match the observed deposition rates both in magnitude and downstream trend. Equation (15) shows the stream-wise decay in deposition rate to be a function of the distance from the inlet, x, normalized by an advection length scale of suspended sediment, $l_a \equiv \frac{q}{r_0 w_s}$. The advective length scale describes the average downstream distance a particle is transported before settling to the bed (Fig. 12). In other words, $l_a = Ut_s$, where U is the depth-average downstream velocity, $t_s = \frac{H_s}{w_s}$ is the average particle settling time, and $H_s = h/r_0$ is the average particle fall distance (Fig. 12). It shows that larger discharge flows can advect sediment of a particular size farther downstream. An advection length scale of settling sediment has been derived previously and shown to be important in bedform stability (Fredsøe and Deigaard, 1992; Mohrig and Smith, 1996), tsunami deposition (Moore et al., 2007), and turbidity currents (Dade and Huppert, 1994; Straub and Mohrig, 2008).

Equation (15) predicts that, if entrainment of sediment from the bed is negligible, larger discharge flows can maintain higher sediment concentrations and higher deposition rates over greater distances, and this is consistent with our observations (Fig. 5C). Furthermore, Equation (15) predicts that the deposition rate is linearly dependent on the inlet sediment concentration, which also matches our observations of greater deposition rates for flows with larger sediment concentrations (Fig. 6C). Near the inlet where flow velocities were the greatest, however, the predictions greatly overestimate the measured deposition rates, and this is because e was not negligible there.

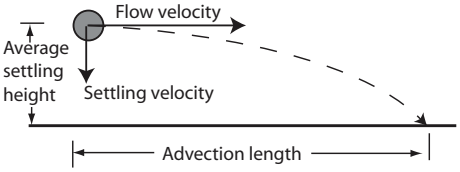

Figure 12. Illustration of an advection length scale of suspended sediment. The advection length is the distance over which an average particle travels downstream before it settles to the bed (e.g., Fredsøe and Deigaard, 1992). The advection length scale is determined by the product of the downstream flow velocity and the settling time, where the settling time is equal to the average height of a particle in the water column divided by the settling velocity.

Equation (15) also predicts that coarser grains with greater settling velocities should have smaller advection lengths resulting in downstream fining, which is consistent with our experiments (Figs. 5D and 6D). The downstream fining was more pronounced for the low discharge case (Fig. 5D) as expected because, for smaller discharges, all grain sizes will have shorter advection length scales resulting in larger stream-wise gradients in median grain size.

IMPLICATIONS AT FIELD SCALE

The goal of our experiments was to evaluate the question posed by Figure 1: Do hyperpycnal-plume deposits track the rising and falling discharge of a river flood? Our experiments have revealed three important findings that related to this problem. First, the criterion used to define a plunging current, that its density is greater than the ambient density, is not sufficient. In addition, the turbid plume must reach a sufficient depth to destabilize. This allows the formation of a depth-limited plume, and deposition within this zone can significantly reduce the sediment concentration at the plunge point. Second, local hyperpycnal-flow velocities can be correlated (outside of the spatial zone affected by plunge-point translation), anticorrelated (within the zone affected by plunge-point translation), or uncorrelated (if river sediment concentration varies independent of discharge) to changes in river-flood discharge. Third, hyperpycnal-flow deposits do not necessarily record plunge-point dynamics and can be partly or completely dominated by fluvial inlet conditions due to a large advection length scale of suspended sediment. Below we discuss the implications of these findings in more detail, as well as potential feedbacks with submarine canyon formation and 3-D effects.

To illustrate the results at field scale in the following sections, we will use q = 5 m^2/s, ρ_w = 1000 kg/m^3, ρ_a = 1026 kg/m^3, R = 1.65, F_{dp} = 0.5, and λ_p = 0.5. For perspective, on medium-sized rivers capable of producing hyperpycnal plumes like the Eel River, California (Imran and Syvitski, 2000; Sommerfield and Wheatcroft, 2007), average discharges per unit width can increase from q = ~0.5 m^2/s to ~50 m^2/s for geologically important floods (Mulder and Syvitski, 1995). The Huanghe River, China, is probably the largest river in the world capable of generating frequent hyperpycnal-flow events (Wright et al., 1986; Wright et al., 1988; Wright et al., 1990), and discharge there has varied from 5 m^2/s to 22 m^2/s (the maximum discharge on record [van Gelder et al., 1994]), and could reach as high as 140 m^2/s for the largest possible floods (Mulder and Syvitski, 1995).

Effect of Deposition on Plunging at Field Scale

The experiments have shown that deposition in the depth-limited plume can reduce the sediment concentration at the plunge point. Therefore, deposition might need to be taken into account when evaluating the concentration that rivers must achieve to produce a plunging plume. Equations (4) and (9) can be combined to assess the necessary fluvial sediment concentration to produce a plunging plume in a seaward deepening basin,

$$c_s = c_p + \frac{(1-\lambda_p)}{S}\frac{d\eta}{dt}\left(\frac{\rho_a}{\Delta\rho g F_{dp}^2 q}\right)^{1/3}, \quad (16)$$

where $\Delta\rho = \rho_w(1 + R_{cp}) - \rho_a$ at the plunge point. In the absence of deposition, Equation (16) with Equation (3) reduces to $c_s = c_p = c_c$, which is the criterion normally used to evaluate the likelihood of rivers to produce plunging flows (Mulder and Syvitski, 1995; Warrick and Milliman, 2003; Hicks et al., 2004; Dadson et al., 2005).

Equation (16) shows that the necessary fluvial sediment concentration can be much larger than the typical value for density equivalence ($c_s = c_p = c_c$ = 1.6%), especially for large deposition rates and small basin slopes (Fig. 13). The trend with slope illustrates the importance of basin geometry and flow depth on plunge dynamics. In a low sloping basin

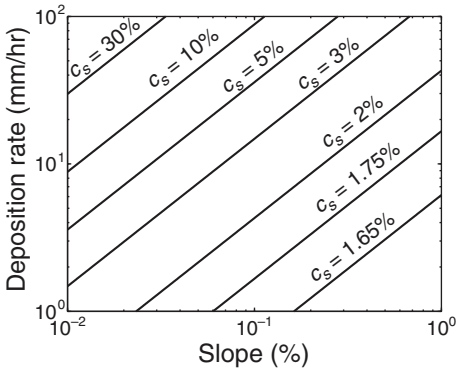

Figure 13. Contours of the necessary fluvial sediment concentration at the river mouth (c_s) to form a plunging hyperpycnal plume as a function of basin slope and deposition rate following Equation (16). For this example, the density of ocean water was set to ρ_a = 1026 kg/m^3, which yields a necessary minimum sediment concentration at the plunge point (for density equivalence) of $c_p = c_c$ = 1.6%. Where deposition is important, the input fluvial sediment concentration would have to be larger than this for plunging to occur.

the plunge point must extend farther seaward to achieve the necessary depth to plunge. This in turn extends the length of the depth-limited plume and the zone over which deposition occurs prior to plunging. If the fluvial sediment concentration is less than that predicted by Equation (16), the depth-limited plume will push seaward across the basin until it dissipates, becomes hypopycnal due to deposition, or reaches the end of the basin. The second scenario can arise in nature because, unlike our flume experiments that used a freshwater basin, deposition can cause turbid freshwater river plumes to become less dense than saline water and rise to the ocean surface (e.g., Sparks et al., 1993; Hogg et al., 1999). The last scenario can arise even if the deposition rate is zero, because, although the current is denser than the ambient fluid, it will never plunge if it does not reach sufficient depth to become unstable.

The necessary fluvial sediment concentration to plunge (Equation 16) is weakly dependent on the fluid discharge. Despite the fact that larger discharge flows push the plunge point farther seaward, increasing the area over which deposition occurs, these flows also advect sediment from the river to the plunge point at a faster rate. Equation (16) indicates that the latter effect is dominant such that larger discharge flows require a lower fluvial sediment concentration to produce a plunging plume.

Plume Dynamics at Field Scale

The conceptual model of Figure 1 predicts that flow velocities in a hyperpycnal plume increase with increasing river discharge. For the experiments with the same sediment concentration, this was true downstream of the maximum extent of plunging (x > 2 m) and upstream of the plunge point in the depth-limited plume (x < 1.5 m) (Fig. 5B). The experiments reveal a more complicated signal near the plunge point, however, where larger discharges produced smaller velocities due to translation of the plunge point.

Although often neglected in hyperpycnal-plume models (e.g., Mulder et al., 1998; Imran and Syvitski, 2000), the offshore region where plume velocities can be anti-correlated with river discharge is large at field scale. The size of this region can be determined by the extent of plunge-point translation during a river flood. Figure 14A shows the predicted plunge-point depth as a function of sediment concentration and discharge following Equation (4) with F_{dp} = 0.5. As discussed above, on rivers like the Eel or Huanghe, discharge can increase substantially during flood from ~0.5 m^2/s to 50 m^2/s or ~5 m^2/s to 140 m^2/s, respectively. These variations in discharge can result in changes in equilibrium plunge-point depth of tens of meters (Fig. 14A). This in turn causes the plunge point to move, for example, by distances of kilometers for a bed slope of S = 1% or tens of kilometers for S = 0.1%. Thus, during substantial river floods at field scale, the region where flow velocities are anti-correlated to the fluvial discharge can extend over many kilometers seaward of the river mouth (Lamb and Mohrig, 2009).

Further complicating the transfer of momentum from a river to its derived turbidity current is the dependence of local velocity on sediment concentration. Unlike changes in discharge, changes in sediment concentration should have no effect on flow velocity within the depth-limited plume. Changes in velocity in this zone must be due to changes in fluvial discharge. However, the sediment concentration partially determines the location of the plunge point and the velocity of the plunging plume and turbidity current (Fig. 14). Our experiments show that an increase in sediment concentration can cause the plunge point to retreat upstream and that velocities will correspondingly increase in the plunging and turbidity current zones (Fig. 6). At field scale, a change in sediment concentration by a few volume percent can change the plunge depth by tens of meters, especially at concentrations near the critical concentration to plunge (Fig. 14A). Again, this can result in translation of the plunge point by kilometers or more depending on the basin slope.

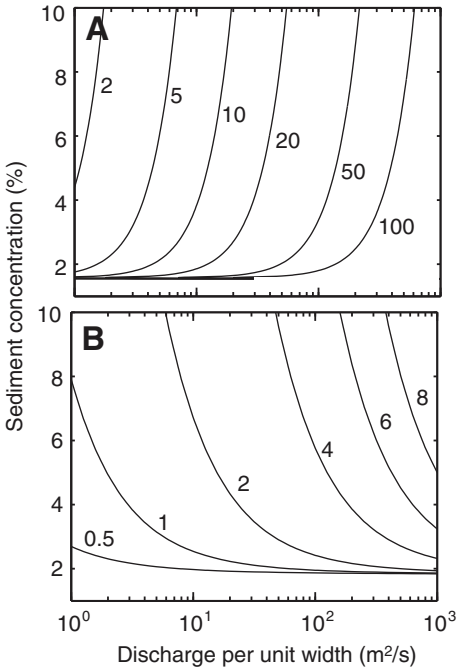

Figure 14. Contours of (A) depth at the plunge point (with units of m) and (B) flow velocity downstream of the plunge zone (with units of m/s) as a function of discharge and volumetric sediment concentration at the river mouth following Equations (4) and (14). These calculations assume no sediment deposition upstream of the plunge point and a critical sediment concentration to plunge of 1.6%.

During a river flood, sediment concentration typically increases with discharge, although this relationship can be complex (e.g., Mulder and Syvitski, 1995; Topping et al., 2000a; Topping et al., 2000b). Depending on the temporal history of sediment concentration and discharge through the duration of a flood event, the plunge point could advance or retreat as discharge increases. Within the zones affected by migration of the plunge point, this can result in a complex sequence of multiple flow accelerations and decelerations even during a single peaked flood event (Lamb and Mohrig, 2009).

Plume Deposits at Field Scale

In the experiments it was found that the deposits did not accurately record the translation of the plunge point. Instead, the deposits generally fined and thinned downstream, and changes in deposition rate and grain size were correlated to changes in inlet discharge and sediment concentration. This finding is encouraging. It shows that despite the complexity of plunge-point

dynamics, hyperpycnal-plume deposits might still contain a decipherable record of the temporal evolution of river discharge and sediment concentration during flood events. In the experiments the strong influence of inlet conditions occurred because entrainment of sediment was negligible (away from the inlet), and the advection of sediment was significant. It is necessary to evaluate if and when this might also be the case in natural systems.

To investigate this, it is useful to rewrite the sediment continuity equation (Equation 10) in terms of sediment flux and use a scaling analysis to identify the dominant terms. To make this transformation, the sediment flux per unit width can be defined as $q_s \equiv cq$ for suspended sediment. The sediment transport capacity per unit width is $q_{sc} = eq/r_0$ because, where at capacity, the deposition rate is zero, and $e = c_b$ in Equation (10). Rearranging Equation (10) and adding these definitions produces

$$l_a \frac{dq_s}{dx} = q_{sc} - q_s. \quad (17)$$

Thus, the advection length scale $l_a = \frac{q}{r_0 w_s}$ emerges as an important parameter in the sediment continuity equation. In a settling dominated system (small discharges and coarse sediment), $l_a \to 0$ (Fig. 12), and Equation (17) reduces to $q_s = q_{sc}$, a common approximation for bedload sediment transport. For this end-member case, the sediment flux at any specific location on the seabed follows the local transport capacity at the same location, which in turn is a function of local flow dynamics, such as movement of the plunge point. On the opposite end of the spectrum is an advection-dominated depositional system (large discharges and fine sediment), where $l_a \to \infty$, and Equation (17) reduces to $\frac{dq_s}{dx} = 0$, or $q_s = q_{s0}$ after integration, where q_{s0} is the inlet sediment flux per unit width. For this end-member case, the sediment flux at any specific location on the seabed follows the sediment flux at the inlet boundary (e.g., the river mouth) and is insensitive to changes in local transport capacity associated with local decelerations and accelerations of the flow (e.g., due to plunge-point dynamics). The scaling analysis for large l_a is only applicable for depositional systems because it implicitly assumes that q_{sc} does not grow arbitrarily large when $l_a \to \infty$, which must be the case for net deposition (i.e., $q_{sc} \le q_s$).

In natural depositional systems l_a is neither zero nor infinity such that both advection and settling play a role in deposition. We hypothesize that the relative importance of inlet boundary conditions to local flow dynamics can be determined by comparing the length scale of the phenomenon of interest (L) to the advection length scale of sediment (l_a). For example, processes that occur over distances smaller than the advection length scale ($L << l_a$) should not be recorded directly in the deposit because sediment is advected through the region of interest before sediment can settle and interact with the bed (Fig. 15). On the other hand, if the advection length scale is small compared to the length scale of the process of interest ($L >> l_a$), then this process has the potential to be recorded in the deposit.

In our experiments, the inlet discharge ranged from 1×10^{-3} to 4×10^{-3} m^2/s, the settling velocity was 4.4×10^{-4} m/s, and r_0 was ~1.5. Thus, the advection length scale $l_a = \frac{q}{r_0 w_s}$ was on the order of 1.5–6 m for the different experiments. The stream-wise length of the plunging zone and the movement of the plunge point in response to changing discharge, however, was ≤0.5 m. This suggests that $L < l_a$ in our experiments and the suspended sediment did not have time to interact with the bed within the plunge zone due to its downstream advection. Thus, the deposits in our experiment should have been insensitive to plunge-point dynamics (Fig. 15), which appears to be the case (Figs. 5C and 6C).

For natural systems, the advection length scale is much larger than in the flume experiments due to larger discharge flows. For example, with a modest discharge of 5 m^2/s, the same median sediment size as in the experiments would have an advection length scale of l_a = 7.5 km (Fig. 15). This length scale is probably similar to the translation distance of the plunge point during a flood event in natural systems, which can be kilometers or more as discussed previously. Thus, events with finer sediment (e.g., silt and clay) and larger discharges probably have an advection length scale that exceeds the plunge-point translation length during the rising and falling discharge of a flood event (i.e., $L << l_a$). It is these conditions that are most likely to preserve the history of river discharge and sediment concentration in hyperpycnal-plume deposits because they are not sensitive to plunge-point dynamics.

In contrast, very fine sand ($w_s = 9 \times 10^{-3}$ m/s) in a natural scale flow (e.g., q_0 = 5 m^2/s) would have a much shorter advection length scale of l_a = 300 m, which is probably small compared to the translation distance of the plunge point during a flood event (Fig. 15). These deposits would be substantially different than our experimental findings of beds that fined and thinned downstream with no record of plunge-point dynamics. Instead, deposition rates and particle sizes within the zone of the seabed affected by plunge-point translation might be anti-correlated to changes in river discharge because of plunge-point translation. Local velocity changes caused by translation of the plunge point could be ~0.1 m/s or more (Fig. 14B), which is sufficient to cross bedform stability fields (e.g., ripples to upper plane-bed) for a sandy bed (Southard, 1991; van den Berg and van Gelder, 1993). This suggests that hyperpycnal-flow deposits, and especially the sand fraction, might contain multiple, stacked reverse-to-normally graded beds or sedimentary structures that record multiple flow accelerations and decelerations even from a single-peaked flood event. This is in contrast to the leading hypothesis illustrated in Figure 1 that hyperpycnal-plume deposits record directly the history of discharge at the river mouth.

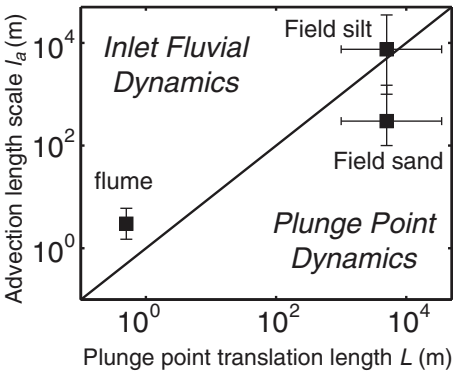

Figure 15. Plot of the advection length scale of settling sediment (l_a) versus the plunge-point translation length (L). We hypothesize that hyperpycnal-flow deposits will record directly river-flood dynamics if $l_a >> L$ and local plunge-point dynamics if $L >> l_a$. Estimates of the two length scales are shown for the flume experiments presented herein, and a field scale hyperpycnal flow depositing silt-sized particles and sand-sized particles (see text for details).

Submarine Canyon Formation

Entrainment of sediment from the bed should be important at field scale since the entrainment rate scales nonlinearly with flow velocity (Smith and Mclean, 1977; García and Parker, 1991). In fact, hyperpycnal flows might erode the seabed, which offers a potentially interesting feedback between plunging hyperpycnal flows and submarine canyon formation (e.g., Pratson et al., 1994). In order for a current to plunge, it must reach sufficient depth to become unstable. The edge of the continental slope offers one of the most abrupt changes in slope, where the water depth dramatically increases downstream. The

result is that most hyperpycnal plumes would be forced to plunge at this slope break or further upstream. Furthermore, the plunging zone is the region of a hyperpycnal plume most likely to cause erosion due to flow acceleration. This erosion could lead to focused retreat of the continental slope forming a submarine canyon. Possibly, as the canyon head cuts landward, it will shorten the length that depth-limited plumes must traverse, driving a greater frequency of plunging within the canyon head and furthering canyon-head retreat.

Three-Dimensional Effects

One of the biggest limitations of our experiments is that the plumes were confined to a 2-D chute and were not allowed to spread laterally. This makes them most applicable to plunging within a submarine canyon or fjord (e.g., Syvitski and Schafer, 1996; Mulder et al., 1998). A laterally spreading plume will decelerate more rapidly, allowing it to reach the plunging criterion (F_{dp} = 0.5) at a shallower depth. This should reduce the translation response of the plunge point to changes in discharge and sediment concentration. The dynamics of a laterally spreading plume depend on the width of the river mouth, spreading angle, bed topography, and mixing along the boundaries (Johnson et al., 1987; Kassem et al., 2003). For a fresh turbid plume entering a saline ocean, mixing along the boundaries could increase the density of the plume and therefore lower the necessary sediment concentration to plunge. Mixing of salty ambient water into freshwater turbidity currents can affect their dynamics (e.g., McLeod et al., 1999), and these affects were not incorporated in our experiments because we used a freshwater basin. Incorporating spreading and mixing is beyond the scope of this paper but should be the focus of future theoretical and experimental work.

CONCLUSIONS

Experimental, turbid hyperpycnal plumes entering a downstream deepening basin plunged where they reached sufficient depth to become unstable. The plunge point corresponded to the position where the flow attained a densimetric Froude number of F_d = 0.5 and the flow collapsed to a F_d value near unity. The depth constraint on plunging allowed for the formation of a depth-limited plume upstream of the plunge point. Deposition within the depth-limited plume reduced the depth-averaged concentrations at the plunge point by as much as half of the fluvial input concentration. Translation of the plunge point in response to changes in fluvial discharge and sediment concentration significantly affected local flow velocities. An increase in fluvial discharge or decrease in sediment concentration forced the plunge point basinward to deeper water. The result was that flow velocities at certain seabed locations were correlated, uncorrelated, and even anti-correlated to changes in fluvial discharge. Despite this complexity, the experimental hyperpycnal-flow deposits were more sensitive to changes in fluvial discharge and sediment concentration than plunge-point dynamics because the advection length scale of suspended sediment, l_a, was large compared to the translation length of the plunge point, L. In natural systems, however, the opposite might be true ($L >> l_a$), especially for sand, in which case hyperpycnal-plume deposits within the zone affected by plunge-point translation can record multiple flow accelerations and decelerations even during a simple single-peaked flood hydrograph. Our results suggest that it is the finest sediments (mud) that are most likely to preserve discharge variations during river-flood events.

ACKNOWLEDGMENTS

We thank Estefania Lazo-Herencia for assisting with the experiments and grain-size analysis, Jim Buttles and Tim Shin for helping with the flume design and instrumentation, and Chris Paola for constructive discussions. Jan Alexander, Chris Paola, and Octavio Sequerios provided helpful formal reviews that strengthened the final manuscript. Funding for this project was provided by the RioMAR Industrial Consortium and the Jackson School of Geosciences, University of Texas–Austin.

APPENDIX: NOTATION

c—Depth-averaged volumetric sediment concentration.
c_b—Near-bed volumetric sediment concentration.
c_0—Depth-averaged volumetric sediment concentration at the inlet.
c_c—Critical depth-averaged volumetric sediment concentration to plunge.
c_d—Depth-averaged sediment concentration downstream of plunging.
c_p—Depth-averaged sediment concentration at the plunge point.
D_{16}—Grain size in which 16% of the sample is finer.
D_{50}—Median grain size.
D_{50d}—Depth-averaged median grain size in the flow downstream of plunging.
D_{50p}—Depth-averaged median grain size in the flow at the plunge point.
D_{84}—Grain size in which 84% of the sample is finer.
e—Dimensionless entrainment parameter of bed sediment.
F_d—Densimetric Froude number.
F_{dd}—Densimetric Froude number at the downstream boundary of the plunge zone.
F_{dp}—Densimetric Froude number at the plunge point.
g—Acceleration due to gravity.
h—Depth of turbid flow.
h_d—Flow depth downstream of plunging.
h_p—Flow depth at the plunge point.
H_s—Average particle fall height.
l_a—Advection length scale of settling sediment.
L—Length scale of plunge-point translation during a river flood.
L_p—Length of the plunge zone.
q—Volumetric discharge of turbid flow per unit width.
q_0—Volumetric discharge of turbid flow per unit width at the inlet.
q_d—Volumetric discharge of turbid flow per unit width downstream of plunging.
q_p—Volumetric discharge of turbid flow per unit width at the plunge point.
q_s—Volumetric discharge of suspended sediment per unit width.
q_{s0}—Volumetric discharge of suspended sediment per unit width at the inlet.
q_{sc}—Volumetric sediment transport capacity per unit width.
r_0—Dimensionless ratio of near-bed to depth-averaged sediment concentration.
R—Submerged specific density of sediment.
S—Bed slope.
t—Time.
t_s—Average particle settling time.
U—Depth-averaged velocity.
w_s—Settling velocity of sediment.
x—Stream-wise coordinate.
x_d—Stream-wise location of the downstream boundary of the plunge zone.
x_p—Stream-wise location of the plunge point.
x_s—Stream-wise location of the shoreline or inlet.
β—Bed slope angle.
γ—Dimensionless coefficient of mixing in the plunge zone.
η—Elevation of the sediment bed.
λ_p—Bed porosity.
$\Delta\rho$—Density difference between the plume and ambient fluid.
ρ_a—Density of the ambient fluid.
ρ_s—Density of sediment.
ρ_w—Density of freshwater.

REFERENCES CITED

Akiyama, J., and Stefan, H.G., 1984, Plunging flow into a reservoir—Theory: Journal of Hydraulic Engineering, v. 110, no. 4, p. 484–499, doi: 10.1061/(ASCE)0733-9429(1984)110:4(484).

Best, J.L., Kostaschuk, R.A., Peakall, J., Villard, P.V., and Franklin, M., 2005, Whole flow field dynamics and velocity pulsing within natural sediment-laden underflows: Geology, v. 33, p. 765–768, doi: 10.1130/G21516.1.

Dade, B.W., and Huppert, H.E., 1994, Predicting the geometry of channelized deep-sea turbidites: Geology, v. 22, p. 645–648, doi: 10.1130/0091-7613(1994)022<0645:PTGOCD>2.3.CO;2.

Dadson, S., Hovius, N., Pegg, S., Dade, W. B., and Horng, M. J., 2005, Hyperpycnal river flow from an active mountain belt: Journal of Geophysical Research, v. 110, no. F04016, doi: 10.1029/2004JF000244.

Dai, A., and Garcia, M.H., 2009, Discussion of "Note on the analysis of plunging density flows" by Gary Parker and Horacio Toniolo: Journal of Hydraulic Engineering, v. 135, p. 532–533, doi: 10.1061/(ASCE)HY.1943-7900.0000005.

Farrell, G.J., 1986, Buoyancy induced plunging flow into reservoirs and coastal regions [Ph.D. thesis]: University of Minnesota.

Federal Interagency Sedimentation Project, 1941, Laboratory Investigation of Suspended Sediment Samplers, Interagency Report 5: Iowa City, Iowa, University of Iowa Hydraulics Laboratory, 99 p.

Felix, M., Peakall, J., and McCaffrey, W.D., 2006, Relative importance of processes that govern the generation of particulate hyperpycnal flows: Journal of Sedimentary Research, v. 76, no. 1–2, p. 382–387, doi: 10.2110/jsr.2006.022.

Fredsøe, J., and Deigaard, R., 1992, Mechanics of Coastal Sediment Transport, Advanced Series on Ocean Engineering, Volume 3: Singapore, New Jersey, World Scientific, 369 p.

Garcia, M., 1994, Depositional turbidity currents laden with poorly sorted sediment: Journal of Hydraulic Engineering, v. 120, p. 1240–1263, doi: 10.1061/(ASCE)0733-9429(1994)120:11(1240).

García, M.H., and Parker, G., 1991, Entrainment of bed sediment into suspension: Journal of Hydraulic Engineering, v. 117, no. 4, p. 414–435, doi: 10.1061/(ASCE)0733-9429(1991)117:4(414).

Henderson, F.M., 1966, Open Channel Flow: New York, Macmillan, 522 p.

Hicks, D.M., Gomez, B., and Trustrum, N.A., 2004, Event suspended sediment characteristics and the generation of hyperpycnal plumes at river mouths: East Coast Continental Margin, North Island, New Zealand: The Journal of Geology, v. 112, no. 4, p. 471–485, doi: 10.1086/421075.

Hogg, A.J., Huppert, H.E., and Hallworth, M.A., 1999, Reversing buoyancy of particle-driven gravity currents: Physics of Fluids, v. 11, p. 2891–2900, doi: 10.1063/1.870147.

Imran, J., and Syvitski, J.P.M., 2000, Impact of extreme river events on the coastal ocean: Washington, D.C., Oceanography, v. 13, p. 85–92.

Itakura, T., and Kishi, T., 1979, Study of the turbidity current in a reservoir: Proceedings of the 16th Symposium, Science of Natural Disasters, p. 233–234.

Johnson, K.S., Paull, C.K., Barry, J.P., and Chavez, F.P., 2001, A decadal record of underflows from a coastal river into the deep sea: Geology, v. 29, no. 11, p. 1019–1022, doi: 10.1130/0091-7613(2001)029<1019:ADROUF>2.0.CO;2.

Johnson, T.R., Farrell, G.J., Ellis, C.R., and Stefan, H.G., 1987, Negatively buoyant flow in a diverging channel. 1: Flow regimes: Journal of Hydraulic Engineering, v. 113, no. 6, p. 716–730.

Kassem, A., Imran, J., and Khan, J.A., 2003, Three-dimensional modeling of negatively buoyant flow in diverging channels: Journal of Hydraulic Engineering, v. 129, no. 12, p. 936–947, doi: 10.1061/(ASCE)0733-9429(2003)129:12(936).

Kineke, G.C., Woolfe, K.J., Kuehl, S.A., Milliman, J.D., Dellapenna, T.M., and Purdon, R.G., 2000, Sediment export from the Sepik River, Papua New Guinea: Evidence for a divergent sediment plume: Continental Shelf Research, v. 20, no. 16, p. 2239–2266, doi: 10.1016/S0278-4343(00)00069-8.

Lamb, M.P., Hickson, T., Marr, J.G., Sheets, B., Paola, C., and Parker, G., 2004, Surging versus continuous turbidity currents: Flow dynamics and deposits in an experimental intraslope minibasin: Journal of Sedimentary Research, v. 74, no. 1, p. 148–155, doi: 10.1306/062103740148.

Lamb, M.P., Myrow, P.M., Lukens, C., Houck, K., and Strauss, J., 2008, Deposits from wave-influenced turbidity currents: Pennsylvanian Minturn Formation, Colorado, USA: Journal of Sedimentary Research, v. 78, no. 7–8, p. 480–498, doi: 10.2110/jsr.2008.052.

Lamb, M.P., and Mohrig, D., 2009, Do hyperpycnal flow deposits record river flood dynamics?: Geology, v. 37, no. 12, p. 1067–1070, doi: 10.1130/G30286A.1.

Lee, H.Y., and Yu, W.S., 1997, Experimental study of reservoir turbidity current: Journal of Hydraulic Engineering, v. 123, no. 6, p. 520–528, doi: 10.1061/(ASCE)0733-9429(1997)123:6(520).

McLeod, P., Carey, S., and Sparks, R.S.J., 1999, Behavior of particle-laden flows in the ocean: Experimental simulation and geological implications: Sedimentology, v. 46, p. 523–536, doi: 10.1046/j.1365-3091.1999.00229.x.

Mohrig, D., and Smith, J.D., 1996, Predicting the migration rates of subaqueous dunes: Water Resources Research, v. 32, p. 3207–3217, doi: 10.1029/96WR01129.

Moore, A.L., McAdoo, B.G., and Ruffman, A., 2007, Landward fining from multiple sources in a sand sheet deposited by the 1929 Grand Banks tsunami, Newfoundland: Sedimentary Geology, v. 200, p. 336–346, doi: 10.1016/j.sedgeo.2007.01.012.

Mulder, T., and Syvitski, J.P.M., 1995, Turbidity currents generated at river mouths during exceptional discharges to the world oceans: The Journal of Geology, v. 103, p. 285–299, doi: 10.1086/629747.

Mulder, T., Syvitski, J.P.M., and Skene, K.I., 1998, Modeling of erosion and deposition by turbidity currents generated by river mouths: Journal of Sedimentary Research, v. 68, no. 1, p. 124–137.

Mulder, T., Migeon, S., Savoye, B., and Faugeres, J.C., 2001a, Inversely graded turbidite sequences in the deep Mediterranean: A record of deposits from flood-generated turbidity currents?: Geo-Marine Letters, v. 21, no. 2, p. 86–93, doi: 10.1007/s003670100071.

Mulder, T., Migeon, S., Savoye, B., and Jouanneau, J.M., 2001b, Twentieth century floods recorded in the deep Mediterranean sediments: Geology, v. 29, no. 11, p. 1011–1014, doi: 10.1130/0091-7613(2001)029<1011:TCFRIT>2.0.CO;2.

Mulder, T., Syvitski, J.P.M., Migeon, S., Faugeres, J.C., and Savoye, B., 2003, Marine hyperpycnal flows: Initiation, behavior and related deposits: A review: Marine and Petroleum Geology, v. 20, no. 6–8, p. 861–882, doi: 10.1016/j.marpetgeo.2003.01.003.

Myrow, P.M., Lukens, C., Lamb, M.P., Houck, K., and Strauss, J., 2008, Dynamics of a transgressive prodeltaic system: Implications for geography and climate within a Pennsylvanian intracratonic basin, Colorado, USA: Journal of Sedimentary Research, v. 78, no. 7–8, p. 512–528, doi: 10.2110/jsr.2008.061.

Normark, W.R., Posamentier, H., and Mutti, E., 1993, Turbidite systems: State of the art and future directions: Reviews of Geophysics, v. 31, p. 91–116.

Parker, G., and Toniolo, H., 2007, Note on the analysis of plunging of density flows: Journal of Hydraulic Engineering, v. 133, no. 6, p. 690–694, doi: 10.1061/(ASCE)0733-9429(2007)133:6(690).

Parker, G., Garcia, M., Fukushima, Y., and Yu, W., 1987, Experiments on turbidity currents over an erodible bed: Journal of Hydraulic Research, v. 25, p. 123–147.

Parsons, J.D., Bush, J.W.M., and Syvitski, J.P.M., 2001, Hyperpycnal plume formation from riverine outflows with small sediment concentrations: Sedimentology, v. 48, no. 2, p. 465–478, doi: 10.1046/j.1365-3091.2001.00384.x.

Pratson, L.F., Ryan, W.B.F., Mountain, G.S., and Twichell, D.C., 1994, Submarine canyon initiation by downslope-eroding sediment flows: Evidence in late Cenozoic strata on the New Jersey continental slope: Geological Society of America Bulletin, v. 106, p. 395–412, doi: 10.1130/0016-7606(1994)106<0395:SCIBDE>2.3.CO;2.

Smith, J.D., and Mclean, S.R., 1977, Spatially averaged flow over a wavy surface: Journal of Geophysical Research, v. 82, no. 12, p. 1735–1746, doi: 10.1029/JC082i012p01735.

Sommerfield, C.K., and Wheatcroft, R.A., 2007, Late Holocene sediment accumulation on the northern California shelf: Oceanic, fluvial and anthropogenic influences: Geological Society of America Bulletin, v. 119, no. 9–10, p. 1120–1134, doi: 10.1130/B26019.1.

Southard, J.B., 1991, Experimental-determination of bedform stability: Annual Review of Earth and Planetary Sciences, v. 19, p. 423–455, doi: 10.1146/annurev.ea.19.050191.002231.

Sparks, R.S.J., Bonnecaze, R.T., Huppert, H.E., Lister, J.R., Hallworth, M.A., Mader, H., and Phillips, J.C., 1993, Sediment-laden gravity currents with reversing buoyancy: Earth and Planetary Science Letters, v. 114, p. 243–257, doi: 10.1016/0012-821X(93)90028-8.

Straub, K.M., and Mohrig, D., 2008, Quantifying the morphology and growth of levees in aggrading submarine channels: Journal of Geophysical Research, v. 113, doi: 10.1029/2007JF000896.

Syvitski, J.P.M., and Schafer, C.T., 1996, Evidence for an earth-quake triggered basin collapse in Saguenay Fjord, Canada: Sedimentary Geology, v. 104, p. 127–153, doi: 10.1016/0037-0738(95)00125-5.

Toniolo, H., Parker, G., and Voller, V., 2007, Role of ponded turbidity currents in reservoir trap efficiency: Journal of Hydraulic Engineering, v. 133, no. 6, doi: 10.1061/(ASCE)0733-9429(2007)133:6(579).

Topping, D.J., Rubin, D.M., Nelson, J.M., Kinzel, P.J., and Corson, I.C., 2000a, Colorado River sediment transport—2. Systematic bed-elevation and grain-size effects of sand supply limitation: Water Resources Research, v. 36, no. 2, p. 543–570, doi: 10.1029/1999WR900286.

Topping, D.J., Rubin, D.M., and Vierra, L.E., 2000b, Colorado River sediment transport—1. Natural sediment supply limitation and the influence of Glen Canyon Dam: Water Resources Research, v. 36, no. 2, p. 515–542, doi: 10.1029/1999WR900285.

Turner, J.S., 1973, Buoyancy Effects in Fluids: London, Cambridge University Press, 368 p.

van den Berg, J.H., and van Gelder, A., 1993, A new bedform stability diagram, with emphasis on the transition of ripples to plane bed in flows over fine sand and silt: Special Publication of the International Association of Sedimentologists, v. 17, p. 11–21.

van den Berg, J.H., van Gelder, A., and Mastbergen, D.R., 2002, The importance of breaching as a mechanism of subaqueous slope failure in fine sand: Sedimentology, v. 49, p. 81–95, doi: 10.1046/j.1365-3091.2002.00433.x.

van Gelder, A., van den Berg, J.H., Cheng, G., and Xue, C.T., 1994, Overbank and channelfill deposits of the modern Yellow River Delta: Sedimentary Geology, v. 90, no. 3–4, p. 293–305, doi: 10.1016/0037-0738(94)90044-2.

Warrick, J.A., and Milliman, J.D., 2003, Hyperpycnal sediment discharge from semiarid southern California rivers: Implications for coastal sediment budgets: Geology, v. 31, no. 9, p. 781–784, doi: 10.1130/G19671.1.

Winterstein, T.A., and Stefan, H.G., 1983, Suspended sediment sampling in flowing water: laboratory study of the effects of nozzle orientation withdrawal rate and particle size: External Memorandum M-168, Saint Anthony Falls Laboratory, University of Minnesota, 97 p.

Wright, L.D., Yang, Z.S., Bornhold, B.D., Keller, G.H., Prior, D.B., and Wiseman, W.J., 1986, Hyperpycnal plumes and plume fronts over the Huanghe (Yellow River) Delta Front: Geo-Marine Letters, v. 6, no. 2, p. 97–105, doi: 10.1007/BF02281645.

Wright, L.D., Wiseman, W.J., Bornhold, B.D., Prior, D.B., Suhayda, J.N., Keller, G.H., Yang, Z.S., and Fan, Y.B., 1988, Marine dispersal and deposition of Yellow-River silts by gravity-driven underflows: Nature, v. 332, no. 6165, p. 629–632, doi: 10.1038/332629a0.

Wright, L.D., Wiseman, W.J., Yang, Z.S., Bornhold, B.D., Keller, G.H., Prior, D.B., and Suhayda, J.N., 1990, Processes of marine dispersal and deposition of suspended silts off the modern mouth of the Huanghe (Yellow River): Continental Shelf Research, v. 10, no. 1, p. 1–40, doi: 10.1016/0278-4343(90)90033-I.

Manuscript Received 7 July 2009
Revised Manuscript Received 17 November 2009
Manuscript Accepted 30 November 2009

Printed in the USA